Talanta 94 (2012) 328–334

Contents lists available at SciVerse ScienceDirect

Talanta

journal homepage: www.elsevier.com/locate/talanta

Influence of macroporous gold support and its functionalization on lactate oxidase-based biosensors response

M. Gamero[a], M. Sosna[c], F. Pariente[b], E. Lorenzo[b], P.N. Bartlett[c], C. Alonso[a,*]

[a] Department of Applied Physical Chemistry, Universidad Autónoma de Madrid, 28049 Madrid, Spain
[b] Department of Analytical Chemistry, Universidad Autónoma de Madrid, 28049 Madrid, Spain
[c] School of Chemistry, University of Southampton, SO17 1BJ, UK

ARTICLE INFO

Article history:
Received 19 December 2011
Received in revised form 6 March 2012
Accepted 20 March 2012
Available online 4 April 2012

Keywords:
Macroporous gold
Lactate oxidase
Biosensor
Modified electrodes

ABSTRACT

A general bioanalytical platform for biosensor applications was developed based on three-dimensional ordered macroporous (3DOM) gold film modified electrodes using lactate oxidase (LOx) as a case study, within the framework of developing approaches of broad applicability. The electrode was electrochemically fabricated with an inverted opal template, making the surface area of the 3DOM gold electrode up to 18 times higher than that of bare flat gold electrodes. These new electrochemical transducers were characterized by using Field Emission Scanning Electron Microscopy (FE-SEM), Atomic Force Microscopy (AFM) and the X-ray diffraction (XRD). The biosensor was developed by immobilization of lactate oxidase (LOx), on a 3DOM gold electrode modified with a self-assembled monolayer of dithiobis-N-succinimidyl propionate (DTSP). The resulting lactate oxidase biosensor was characterized by electrochemical impedance spectroscopy (EIS). The 3DOM gold electrode not only provides a good biocompatible microenvironment but also promotes the increase of conductivity and stability. Thus, the developed lactate oxidase bioanalytical platforms showed higher mediated bioelectrocatalytic activity compared to others previously described based on polycrystalline gold transducers. The response to varying lactate concentrations has been obtained in the presence of hydroxymethylferrocene as redox mediator in solution. Under these conditions, the bioanalytical platform response for DTSP covalently bound enzyme was improved with respect to that obtained in absence of DTSP.

1. Introduction

Biosensors based on flat gold electrode surfaces modified with self-assembled monolayers are widely used, including fundamental studies of electrochemical processes on modified electrodes. For some applications, such as in vivo measurements, it may be necessary to use miniaturized electrodes and smaller active electrode surface will lead to lower analytical response. Therefore, to achieve a sufficiently high rate of electrochemical conversion, the electrode surface area must be increased artificially by using nanostructured [1] or porous materials [2]. An ideal way to develop metallic macroporous materials with controlled size and the spatial arrangement of the pores is to use colloidal crystal films as templates for subsequent electrodeposition [3–5]. Afterwards, the template is removed by an appropriate solvent and highly ordered structures of macroporous metal are obtained [6,7]. Due to its large surface area to volume ratio, this kind of structure can be considered as a good candidate for biosensors. Thus, Xia and co-workers developed a 3DOM gold film modified electrode to study the direct electron transfer of hemoglobin [8,9]. Macroporous ultramicroelectrodes [7], 3DOM Prussian blue film and 3DOM gold film modified electrodes have also been prepared for glucose detection [10,11].

Recently, 3DOM gold film modified electrodes have also been used for immunosensor development [12,13]. In these systems, the sensing enhancement was significantly higher than that of respective nonporous electrodes.

The development of methods for the determination of L-lactic acid is of great importance in several areas such as medicine and food industry [14–20].

Our efforts over the past years in this field have been addressed to design L-lactic acid biosensors based on lactate oxidase (LOx). In the present work, we describe the preparation and characterization of a 3D macroporous gold inverse opal films, using polystyrene colloidal crystals as templates, in order to obtain a nanostructured electrodes that can be used in the design of significantly improved lactate biosensors. To achieve the enzyme immobilization we have employed two strategies: (i) direct adsorption onto the 3D macroporous gold surface and (ii) covalent bonding to 3D gold surfaces

* Corresponding author at: Dto. Química Física Aplicada, Universidad Autónoma de Madrid, C/FranciscoTomás y Valiente 7, 28049 Madrid, Spain. Tel.: +34 4978742; fax: +34 4974785.
E-mail address: concepcion.alonso@uam.es (C. Alonso).

0039-9140/$ – see front matter © 2012 Elsevier B.V. All rights reserved.
http://dx.doi.org/10.1016/j.talanta.2012.03.051

previously modified with a bifunctional reagent containing succinimide functionalities, in particular, 3,3′-dithiodipropionic acid di(N-succinimidyl ester) (DTSP) [19]. The biosensor response was obtained by replacing the natural electron acceptor (O_2) by an artificial mediator (hydroxymethylferrocene, HMF), whose electrochemical behaviour (anodic peak current in cyclic voltammetric response) is followed at −0.16 V, instead of detecting the hydrogen peroxide generated in the lactate oxidation.

This strategy allows minimizing the contribution of interfering substances that could be oxidized at the high potential required for H_2O_2 detection [19,21].

To characterize the morphology and physical properties of the resulting biosensors, microscopic, impedimetric and voltammetric techniques have been used. Their electrocatalytic response has been compared with that obtained under the same conditions using a polycrystalline gold electrode as well as roughened gold electrodes [1].

2. Materials and methods

2.1. Reagents and substrates

The monodisperse polystyrene colloidal spheres solution (500 nm diameter) was obtained from Thermo Scientific as a 1.0 wt% suspension in water. The commercial gold plating solution (ECF 60) containing 10 g/l gold was obtained from Metalor. The gold electrodes used as substrates were prepared by thermal vapor deposition of 10 nm of a chromium adhesion layer, followed by 200 nm of gold, onto standard 1 mm thick glass microscope slides. The gold electrodes were cleaned by sonication in isopropyl alcohol (IPA) for 1 h followed by rinsing with deionized water. Lactate oxidase (EC 232-841-6 from *Pediococcus* species) lyophilized powder containing 41 units/mg solid was obtained from the Sigma Chemical Co. (St. Louis, MO). Stock solution was prepared by dissolving 1.3 mg of the LOx lyophilized powder in 250 μl of 0.1 M, pH 7 phosphate buffer, aliquoted (10 μl) and stored at −30 °C. Under these conditions the enzymatic activities remain stable for several weeks. 0.1 M stock solution of L-(+)lactic acid lithium salt 97% (Sigma) containing 1 mM hydroxymethylferrocene was prepared. 3,3′-dithiodipropionic acid di(N-succinimidyl ester) (DTSP), hydroxymethylferrocene (HMF) and dimethyl-sulfoxide (DMSO) were obtained from Aldrich and used as received. Other chemicals used in this work, such as sulphuric acid and sodium phosphate, were reagent grade quality and used as received without additional purification steps. Sodium phosphate (Merck) was employed for the preparation of buffer solutions (0.1 M, pH 7.0). All the solutions were prepared with ultra pure water by means of a Millipore Milli-Q system (18.2 MΩ cm).

2.2. Instrumentation

2.2.1. Electrochemical cell

The electrochemical measurements were performed in a conventional three-electrode set-up. In the case of catalytic measurements the volume of solution used was 10.0 ml. For 3D macroporous gold biosensor the working electrode was template-coated gold. A large area gold electrode was used as counter electrode. All the potentials are quoted with respect to mercury/mercurous sulphate reference electrode (SMSE). The electroactive surface area of the working electrodes was determined by cyclic voltammetry in 0.50 M H_2SO_4 from the charge under the reduction peak of gold oxide.

A conversion factor of 400 μC cm^{-2} was used [22]. The experiments were performed in solutions thermostated at 25 ± 0.5 °C.

2.2.2. Electrochemical Impedance spectroscopy measurements

EIS experiments were performed with an Autolab PGSTAT 30 potentiostat from Eco-Chemie. The solution was 0.1 M PBS (pH 7), 0.1 M KCl containing 10 mM $K_3Fe(CN)_6$ + 10 mM $K_4Fe(CN)_6$. A sinusoidal potential modulation of ±10 mV amplitude in 10^5–10^{-3} Hz frequency range, spaced logarithmically (120 per 8 decades), was superimposed on the formal potential of the redox couple $[Fe(CN)_6]^{3-/4-}$ (−0.21 V vs. MSE). To obtain the capacitance from the experimental data, the frequency f_i was selected to obtain the maximum value of Z''. The capacitance was calculated as $C = 1/(2\pi f_i R_{CT})$, where R_{CT} is the charge transfer resistance.

EIS results were analysed by fitting the experimental impedance data to Randles equivalent circuit. The electrical equivalent circuit parameters were calculated by fitting the impedance function to the measured spectra with a non-linear least-squares (NLLS) program using *Z*-plot/*Z*-view for all the frequencies measured. The criteria used to estimate the fitting quality were evaluated firstly with the low chi-square value and secondly with the low estimative errors (%) for all the components.

2.2.3. SEM, XRD and AFM characterization

The equipment used for the characterization of template-coated gold and macroporous gold samples was a Philips XL30 Scanning Electron Microscope equipped with a Field Emission Gun (FEG) and coupled with an Energy Dispersive X-ray analyzer (EDX DE4i). The samples were examined at 15 keV acceleration voltages.

For the atomic force microscopy (AFM) studies, a JPK NanoWizard II system was used. Measurements were carried out using silicon nitride cantilevers (Model OCML-RC800PSA; 71 kHz; *k* 0.73 N/m) from Olympus. Tapping mode was used for topographical characterization of the inverse opal gold electrodes electrodeposited on Au/Cr/glass slides as well as for gold electrodeposited on Au/Cr/glass slides prepared under the same conditions of potential and temperature as 3D macroporous gold samples in air. The images were only linearly flattened, in order to account for sample tilt.

The phases present in the coating were determined by X-ray diffractometry (X'Pert PRO XRD, Panalytical) at a glancing angle of 0.5° and 1° using Cu Kα line generated at 40 mA, 45 kV. Start Position [2θ (°)] 30.0200; End Position [2θ (°)] 99.9800; Step Size [2θ (°)] 0.0200; Scan Step Time [s] 2.0000. The measurement of width at half height ($W_{1/2}$) of each of the diffractogram peaks, for the determination of crystallite size, was performed with the X'Pert HighScore Plus program. The diffractometer works with the wavelength of copper, which is 1.5406 nm.

2.3. Procedures

2.3.1. Preparation of macroporous Au electrodes

The method for the self-assembly of the polystyrene (PS) spheres consists basically of the slow evaporation of a small volume of dilute bead suspension (0.05 wt% in water) at the gold substrate surface [23]. To define the geometric area for the electrodeposition step, the electrodes together with the template were coated with a thin varnish film leaving a square window with a desired dimension. The template samples were then put into the commercial gold plating bath (at 25 °C) 5 min prior to the reduction, in order to allow the solution to diffuse all the way throughout the template. Then a potential of −1.05 V vs. SMSE was applied until the required charge had been passed. During the electrodeposition of gold through the template we observed temporal oscillations in the reduction current [6]. These oscillations can be explained by the periodic variation of the active electrode surface area during the growth of gold in the template and they give us an easy and reliable way to control the thickness of the deposit with respect to the number of sphere layers (Fig. 1a).

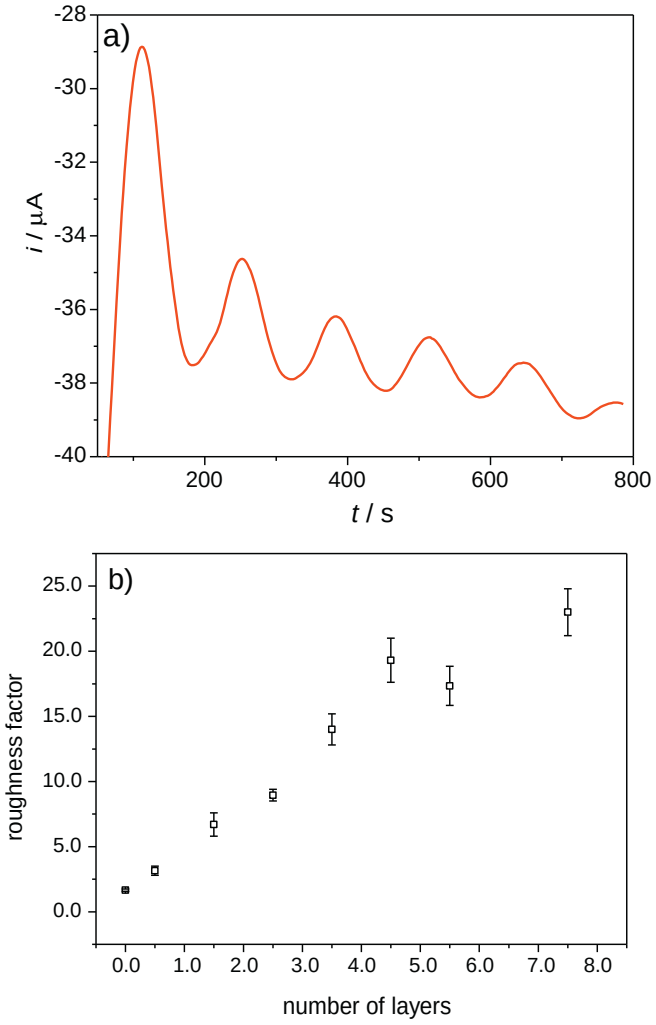

Fig. 1. (a) Typical chronoamperogram obtained for electroplating gold through a 5.5 layers of 500 nm sphere template with a geometric area of 0.06 cm^2. Deposition potential: −1.05 V vs. SMSE. (b) Macroporous gold roughness factor as a function of deposit thickness (expressed as number of template layers).

After the electrodeposition the polystyrene template was removed by dissolving in dimethylformamide in the presence of ultrasound for at least 1 h, leading to the desired macroporous structure with a thickness controllable by the charge used during the electrodeposition step. A linear relationship between the electroactive surface area and the number of layers of hollow spheres was observed (Fig. 1b). For example, in the case of inverse opal with 5.5 sphere layer (used in this work), the roughness factor (R_f) of the 3DOM gold film was calculated to be 18.65, whereas the roughness factor of the bare flat gold electrode was only 1.6.

2.3.2. Biosensor preparation

Macroporous gold electrodes (Au_{3DOM}) were immersed for 3 h at room temperature in a fresh solution of DTSP (4.0 mM in DMSO) to ensure that the whole inner surface was completely modified with a monolayer. The corresponding monolayer containing the active succinimidyl esters was subsequently rinsed in DMSO and 0.1 M, pH 7 phosphate buffer (PB).

10 μl of LOx stock solution was placed on the DTSP-modified macroporous gold electrode. After air-drying, the biosensor was washed with 0.1 M, pH 7 PB to remove any weakly bound enzyme.

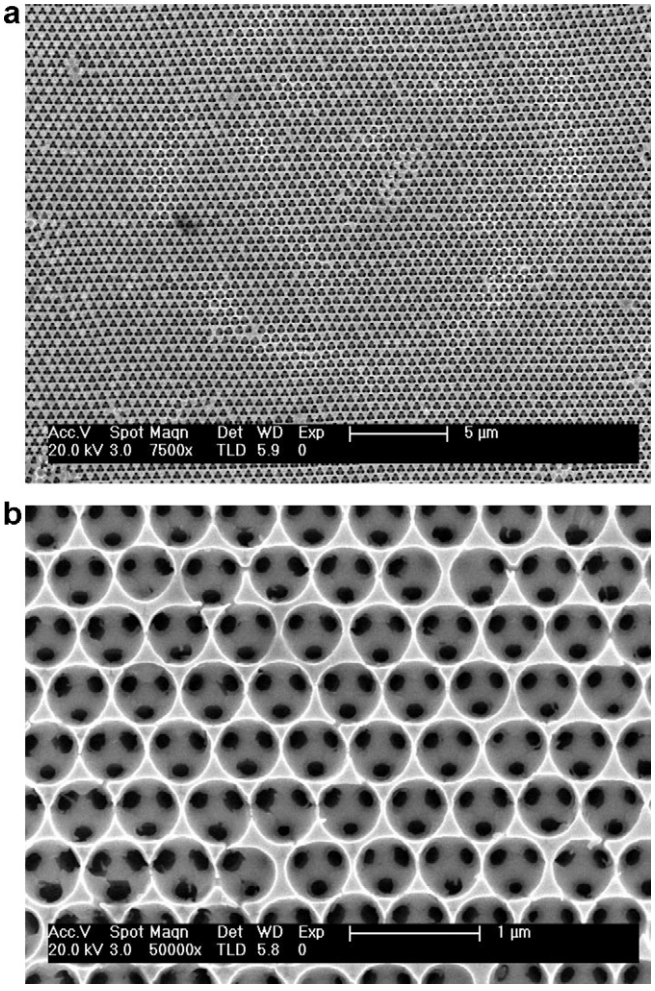

Fig. 2. SEM images of macroporous gold films grown by electrochemical deposition through template assembled from 500 nm diameter polystyrene spheres. (a) Scale 5 μm and (b) scale 1 μm.

3. Results and discussion

3.1. Characterization of 3D macroporous gold electrodes

3.1.1. SEM, AFM and XRD characterization

Fig. 2 shows typical SEM images at different magnifications of the surface of a macroporous gold film grown onto a gold substrate covered with templates made up of 500 nm diameter PS spheres. The SEM images show that the spherical voids left in the gold film after the removal of the PS spheres are arranged in well ordered domains with hexagonal symmetry that can extend over several hundreds of μm^2 (Fig. 2a). Fig. 2b shows a region of a macroporous gold film where the thickness of the film is close to $(n+0.5)\times d$, where d is the diameter of the template sphere. One can clearly observe three small dark circles (diameter ~ 50 nm) within each spherical cavity. These correspond to the interconnecting channels to three spherical voids in the layer below that are formed where the original PS spheres in the two layers were in contact. These interconnections between the spherical voids occur because the electrochemical deposition is unable to completely fill in the narrow regions around the contact points between the separate spheres in the template [24].

The AFM was employed to obtain high resolution images of the 3D macroporous gold transducers (Fig. 3). Although, in principle, the growth of the gold layer is controlled by the current transients, it is possible to observe small areas with different

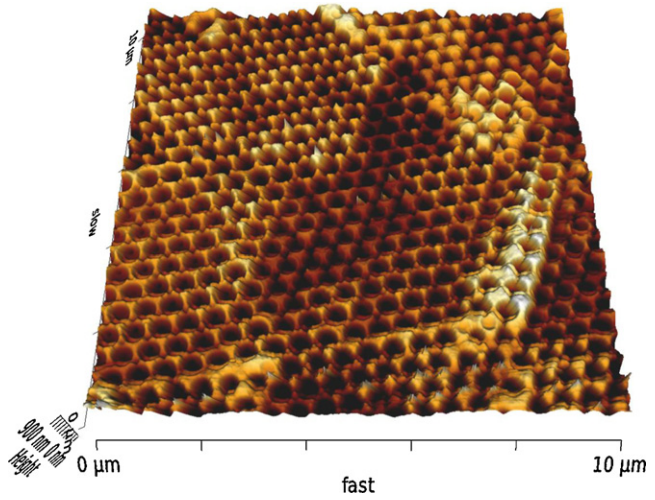

Fig. 3. 10 µm × 10 µm tapping-mode AFM images of macroporous gold films grown by electrochemical deposition through a template assembled from 500 nm diameter polystyrene spheres.

levels of growth. Nevertheless, well ordered domains with hexagonal symmetry over several hundreds of μm^2 were obtained.

Gold crystallizes in the cubic system with $\alpha = \beta = \gamma = 90^\circ$ and $a = b = c = 4.0786$, being the main crystallographic planes (1 1 1), (1 0 0) and (1 1 0). Figure S-1a shows the diffractogram obtained for polycrystalline gold with the X-ray diffraction peak of the greatest intensity corresponding to the orientation (1 1 1). A similar diffractogram is obtained for 3DOM structured Au (Figure S-1b). Calculation of the average crystallite size for the macroporous gold was performed from the X-ray diffraction peak of the greatest intensity, corresponding to orientation (1 1 1). Applying Scherrer's equation [25] an average value of 191 Å is obtained. The average size of the crystallite, for polycrystalline gold, is higher 768 Å.

3.2. Lactate biosensor based on a 3D macroporous gold electrodes

3.2.1. EIS characterization of biosensor development

In the biosensor configuration developed, LOx was either covalently immobilized onto DTSP modified or adsorbed on unmodified 3D macroporous gold transducers. EIS is an effective method for monitoring each step in the construction of biosensor. Fig. 4 shows the impedance changes in the modification process for each one step of Au_{3DOM}-DTSP-LOx biosensor. The Nyquist diagrams of the

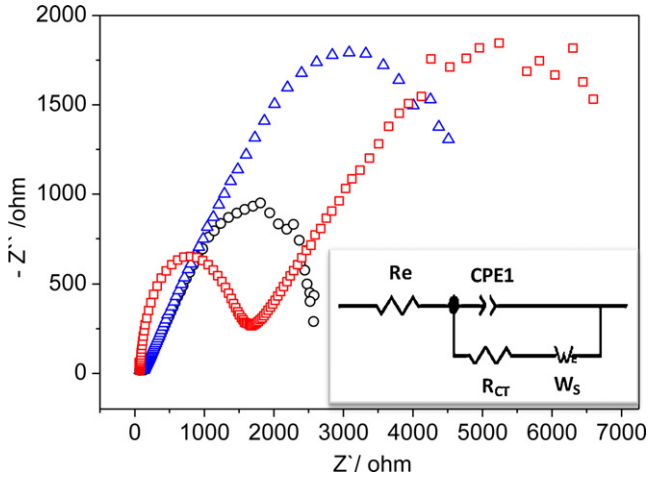

Fig. 4. Nyquist diagram for Au_{3DOM} (○), Au_{3DOM}-DTSP (△) and Au_{3DOM}-DTSP-LOx (□) in PB pH = 7 + 0.1 M KCl containing 10 mM $Fe(CN)_6^{3-}$ + 10 mM $Fe(CN)_6^{4-}$ solution.

Au_{3DOM}, Au_{3DOM}-DTSP and Au_{3DOM}-DTSP-LOx show two frequency regions. At high frequencies (10^4 Hz) the semicircle parts correspond to the charge transfer resistance limiting process associated to either Au_{3DOM}, Au_{3DOM}-DTSP or Au_{3DOM}-DTSP-LOx/electrolyte interface (R_{CT}). The intercept with the real axis, at high frequencies (10^4 Hz), correspond to electrolyte resistance (R_e). At low frequencies the linear part is due to the diffusion process control with the particularity that at very low frequencies, Z' approaches the Warburg resistance (W_S) and Z'' goes to zero. This behaviour is characteristic of diffusion through a finite length diffusion layer.

The impedance diagrams were fitted, considering the Randles equivalent circuit of inset in Fig. 4, which includes the following electronic elements. R_e is the electrolyte resistance between the working and reference electrodes. R_{CT} is the charge transfer resistance—a manifestation of two effects: (1) the energy potential associated with the oxidation event at the electrode (i.e., overpotential), and (2) the redox species energy barrier reaching the electrode due to electrostatic repulsion or steric hindrance. A constant phase element (CPE1) that simulates nonideal behaviour of the capacitor can be modeled as a series by combining the surface modification capacitance and double layer capacitance. R_{CT} and CPE1 correspond to the outer interface (depending on Au_{3DOM} modified or unmodified). W_S is a finite length Warburg element and represents the diffusion through a porous structure of 3DOM gold. In this circuit a distributed element is used instead of a capacitor. Its impedance is $Z = 1/[T(jw)n]$ and is generally used when there is a distribution of relaxation times as a result of inhomogeneities present on the surface.

The experimental results as well as that obtained from the fitting for Au_{3DOM}, Au_{3DOM}-DTSP and Au_{3DOM}-DTSP-LOx are listed in Table 1.

In the first place, the electrolyte resistance values obtained, increase from Au_{3DOM} to Au_{3DOM}-DTSP-LOx. This result could seem wrong since, in principle, the electrolyte resistance should not vary. However, some authors [26] define the resistance Re as a combination of electrolyte resistance between the electrodes and some contribution of film on the electrode surface working. In this sense such increase would be justified.

The 3DOM gold film modified electrode (Au_{3DOM}) reveals a charge transfer resistance (R_{CT}) of 40.21 Ω cm^2 implying, a very low electron-transfer resistance of the redox probe. After the electrode was modified with DTSP, the R_{CT} was slightly bigger. At pH 7.0, the DTSP adsorption onto electrode surfaces creates a negatively charged interface showing self-assembled layer of COO^- terminal groups. Anionic redox markers, such as $[Fe(CN)_6]^{4-/3-}$, are repelled from such interfaces, resulting in inhibition of interfacial electron transfer and an increment of electron transfer resistance (R_{CT} = 81.67 Ω cm^2 vs. R_{CT} = 40.21 Ω cm^2 for the 3DOM gold electrode).

It is possible to relate the magnitude of the charge-transfer resistance to coverage of the electrode by DTSP, assuming that electron-transfer reaction occurs only at bare spots on the electrode surface and that diffusion to these defect sites is planar. If this assumption is correct, it is possible to assuming an equation for the apparent fractional coverage of the electrode based on the charge-transfer resistance of the uncoated electrode [27].

$$\theta = 1 - \frac{R_{CT}^0}{R_{CT}^{SAM}} \quad (1)$$

The DTSP coverage obtained by applying Eq. (1) was 0.51. In principle, this value looks like low but it is necessary to take into account that, there are probably lateral interactions between DTSP molecules in addition to the size of the molecule prevents the charge transfer for $[Fe(CN)_6]^{4-/3-}$ on free sites of the electrode surface.

Table 1
Experimental and fitting results from EIS experiments for 3DOM gold electrode.

	Re (Ω)	R_{CT} (Ω cm^2)	C (F cm^{-2})	W_S (Ω cm^2)	Re (Ω)	R_{CT} (Ω cm^2)	CPE1 (F cm^{-2})	W_S (Ω cm^2)
Au_{3DOM}	44.94	40.21	8.75e−7	1593.51	37.96	45.51	1.61e-5	1673.72
Au_{3DOM}-DTSP	65.99	81.67	1.49e−6	4880.29	71.29	78.24	2.42e-6	5574.42
Au_{3DOM}-DTSP-LOx	74.62	1616.64	2.62e−6	5659.46	76.3	1497.22	3.43e-6	7212.71

After immobilizing LOx covalently, via the reaction of its free amines with the terminal succinimidyl groups of DTSP, the R_{CT} increased again (Table 1). The enzyme forms a superficial layer that difficults the charge transfer between the redox marker in the solution and the electrode surface, due to hindering the diffusion of ferrocyanide toward the electrode surface significantly. The capacities values are consistent with previously observed values [27].

3.2.2. Biosensor response

In the biosensor configuration developed, the immobilized LOx oxidizes L-lactate to pyruvate in the presence of hydroxymethylferrocene (HMF) added to the solution. The electrode acts as a secondary acceptor of electrons, regenerating the redox mediator used in the regeneration of the enzyme, according to the following reaction pathway:

$$\text{l-Lactate} + (\text{LOx})_{ox} \rightarrow \text{pyruvate} + (\text{LOx})_{red} \quad \text{(I)}$$

$$(\text{LOx})_{red} + (\text{HMF})_{ox} \rightarrow (\text{LOx})_{ox} + (\text{HMF})_{red} \quad \text{(II)}$$

$$(\text{HMF})_{red} \rightarrow (\text{HMF})_{ox} + e^- \quad \text{(III)}$$

This sequence of redox events represents a catalytic process. Thus, the magnitude of the catalytic current can be employed as the analytical signal in the determination of the lactate concentration. Fig. 5 illustrates the cyclic voltammetric responses obtained for the 5.5 sphere layer electrodes for either Au_{3DOM}-DTSP-LOx or Au_{3DOM}-LOx in PB (pH 7) containing 1.0 mM hydroxymethylferrocene, in the absence (curves A and C) and in the presence (curves B and D) of substrate. In the absence of substrate, as anticipated, a redox response ascribed to the hydroxymethylferrocene/ferrocenium process is obtained ($E_{pa} - E_{pc} = 73$ mV). Upon addition of lactate, the cyclic voltammogram exhibits an enhancement of the anodic peak current concomitant with a decrease of the cathodic peak current. This behaviour is consistent with a strong electrocatalytic effect and confirms the role of the LOx in the catalytic response to substrate. As a control, either unmodified or modified DTSP macroporous gold electrodes without LOx were immersed in 0.1 M, pH 7.0 PB containing 1.0 mM HMF. In both cases there was no catalysis, i.e. only peaks associated with the ferrocene/ferrocenium process were observed in the absence and in the presence of substrate.

The biosensor response to increasing amount of lactate for both Au_{3DOM}-LOx and Au_{3DOM}-DTSP-LOx based biosensors was obtained from CV experiments. As can be observed in Fig. 6, where efficiency in the catalytic current vs. lactate concentration is plotted, either Au_{3DOM}-LOx or Au_{3DOM}-DTSP-LOx based biosensor show Michaelis–Menten like behaviour, which suggests that in both

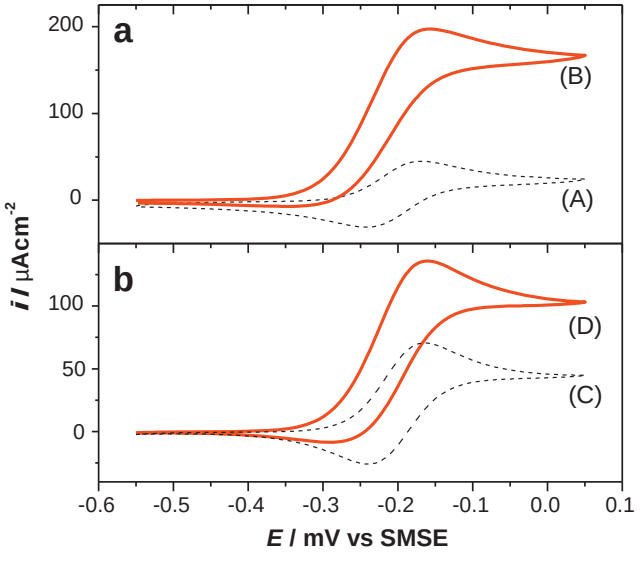

Fig. 5. Cyclic voltammograms for lactate oxidase immobilized onto (a) DTSP-modified macroporous gold electrode (Au_{3DOM}-DTSP-LOx) and (b) unmodified macroporous gold electrode (Au_{3DOM}-LOx), in contact with a 0.1 M, pH 7.0 phosphate buffer solution containing 0.5 mM hydroxymethylferrocene in absence of substrate (curves A and C) and in presence of 14 mM L-lactate (curves B and D). Deposit thickness 5.5 layers ($\nu = 10$ mV s^{-1}).

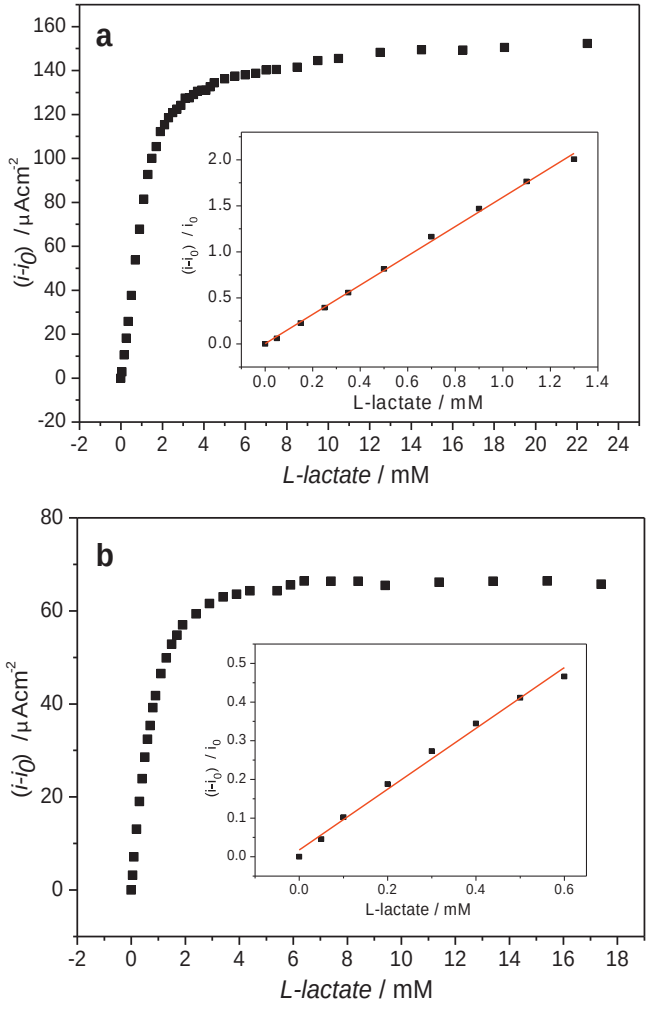

Fig. 6. Calibration curve obtained from peak current in PB pH 7 in presence of increasing amounts of substrate for lactate oxidase immobilized onto (a) a DTSP-modified macroporous gold electrode (Au_{3DOM}-DTSP-LOx) and (b) unmodified (Au_{3DOM}-LOx). Deposit thickness: 5.5 layers (■) experimental data. The inset corresponds to the linear response in each case ($\nu = 10$ mV s^{-1}).

Table 2
Analytical properties of the biosensors built on different nanostructured transducers: rough and macroporous (5.5 layers) gold electrode.

	Au_R-LOx	Au_R-DTSP-LOx	Au_{3DOM}-LOx	Au_{3DOM}-DTSP-LOx
Linear response (mM)	Up to 1.3	Up to 1.2	Up to 0.6	Up to 1.3
K_M (mM)	1.10	0.93	0.62	1.02
I_{MAX} ($\mu A\,cm^{-2}$)	186.3	186.2	65.3	150.0
Sensitivity ($\mu A\,mM^{-1}$)	1.32	1.49	0.79	1.63
Detection limit[a] (μM)	29.82	21.50	16.22	3.93
Determination limit[b] (μM)	99.40	71.81	54.05	13.08
Repeatability[d] (R.S.D.)	0.6%	0.5%	0.5%	0.3%
Reproducibility[c] (R.S.D.)	4.2%	3.9%	3.9%	3.5%
Stability[e]	83%	85%	89%	100%

[a] The detection limit was calculated from the ratio of 3 times the standard deviation of background and the sensitivity.
[b] The determination limit was calculated from 10 times the standard deviation of background current divided by the sensitivity.
[c] The reproducibility was evaluated by comparing the signals obtained using five different biosensors prepared from the same LOx batch for a lactate concentration of 0.5 mM.
[d] The repeatability was evaluated from five measurements of a lactate concentration of 0.5 mM with the same biosensor.
[e] Stability is defined as the percentage of the biosensor signal remaining after one month for three different biosensors.

cases the electrochemical response is under enzymatic control. The experimental data was fitted to a Michaelis–Menten equation by means non-linear regression to calculate the apparent Michaelis–Menten constant K'_M. Values of 0.62 and 1.02 mM were calculated for LOx bound to Au_{3DOM} and Au_{3DOM}-DTSP, respectively. These values indicate that the substrate affinity of the LOx immobilized onto Au_{3DOM}-DTSP surfaces is lower to that observed for LOx immobilized onto Au_{3DOM} surfaces. The increase in the magnitude of K'_M extends the upper limit of the linear response from 0.6 mM for Au_{3DOM}-LOx to 1.3 mM for Au_{3DOM}-DTSP-LOx (see Table 2). The analytical properties of Au_{3DOM}-LOx and Au_{3DOM}-DTSP-LOx were obtained from the insets of Fig. 6. In order to avoid electrode-to-electrode variation we have plotted the normalized response $(i - i_0)/i_0$ vs. the amount of substrate, where i_0 and i represent the current before and after addition of substrate. As can be seen, the sensitivity values, calculated from the slopes of the plots, were 0.79 $\mu A\,mM^{-1}$ (Au_{3DOM}-LOx) and 1.63 $\mu A\,mM^{-1}$ (Au_{3DOM}-DTSP-LOx); indicating again that, as one would expect, the use of DTSP modified surfaces improves the analytical performance. The relative standard deviation for five successive measurements was 0.5% and 0.3% for Au_{3DOM}-LOx and Au_{3DOM}-DTSP-LOx, respectively.

The stability was examined by measuring the response of three different biosensors (prepared with or without DTSP) towards 0.5 mM lactate during one month. When not in use biosensors were stored in PBS at 4 °C. After 30 days, Au_{3DOM}-DTSP-LOx based biosensors retain 100% of its original response, whereas the response of Au_{3DOM}-LOx based biosensors decreases by 11% (Table 2). These results show that the use of DTSP improves significantly the biosensor stability.

As can be seen in Table 2, most of the analytical properties corresponding to the designed biosensors based on macroporous gold electrodes are similar or improved compared to those previously reported by us for other lactate biosensors based on nanostructured rough gold electrodes (Au_R-DTSP-LOx) [1]. In particular, the detection limit (calculated as the ratio between three times the standard deviation of background and the sensitivity) and the determination limit (calculated as the ratio between ten times the standard deviation and the sensitivity) were 3.93 and 13.08 μM, respectively. These values are lower than those (21.50 and 71.81 μM) previously reported for DTSP modified rough gold electrodes (Au_R-DTSP-LOx) based biosensor. Concerning stability, it is significantly improved when macroporous electrodes are used.

Regarding the potential interferents, the Au_{3DOM}-DTSP-LOx biosensor response in presence of several substances, such as tartaric acid, citric acid, ascorbic acid, glucose and fructose was investigated. As one would expect, the results were very similar to those previously observed for Au_R-DTSP-LOx, where these interferents did not affect the biosensor response except for the case of ascorbic acid.

Comparing the analytical performance of the developed lactate biosensing platforms (Au_{3DOM}-DTSP-LOx) to those previously described by us, based on the use of DTSP modified rough gold electrodes (Au_R-DTSP-LOx) (see Table 2), it is clear that the use of gold macroporous electrodes improves the analytical properties of the resulting biosensor, in particular, the sensitivity, detection limit and stability. This improvement is a consequence of the advantages provided by the use of highly ordered macroporous gold with very precise control over the pore size, the spatial arrangement of the pores, and the number of pore layers. These films provide a good microenvironment for the retention of biological activity of the enzyme. In addition its large active surface area allows the immobilization of more protein molecules and the three-dimensional interconnected metallic network provides superior conductivity for electron transfer [8].

4. Conclusions

A comprehensive study of a 3D macroporous gold electrode as a general platform in biosensor development is described. In particular, emphasis has been placed on electrochemical biosensors based on LOx, which was immobilized by covalent binding to these new electrode surfaces modified with DTSP. Different surface characterization techniques (SEM, AFM, XRD) have been employed to characterize this nanostructured surface, which has the advantage of presenting a large specific area and enabling high enzyme loading. As a consequence, the resulting biosensor has improved analytical properties, in particular sensitivity, detection limit and stability with respect to a rough gold electrode. Taking into account the good performance of the presented biosensor, the macroporous gold electrodes are promising transducers for the development of bioanalytical platforms.

Acknowledgements

This work has been supported by the Ministerio de Ciencia y Tecnología of Spain through CTQ2008-05775/BQU Grant and by the Comunidad Autónoma de Madrid (CAM) through AVANSENS S2009/PPQ-1642 Grant.

We would like to thanks Dr. Casado from AFM Service at IMDEA Nanociencia to allow the acquiring of AFM images.

Appendix A. Supplementary data

Supplementary data associated with this article can be found, in the online version, at http://dx.doi.org/10.1016/j.talanta.2012.03.051.

References

[1] M. Gamero, F. Pariente, E. Lorenzo, C. Alonso, Biosens. Bioelectron. 25 (2010) 2038.
[2] S. Ben-Ali, D.A. Cook, P.N. Bartlett, A. Kuhn, J. Electroanal. Chem. 579 (2005) 181.
[3] J.E.G.J. Wijnhoven, S.J.M. Zevenhuizen, M.A. Hendriks, D. Vanmaekelbergh, J.J. Kelly, W.L. Vos, Adv. Mater. (Weinheim, Germany) 12 (2000) 888.
[4] L. Xu, J.B. Wiley, W.L. Zhou, C. Frommen, L. Malkinski, J.-Q. Wang, R.H. Baughman, A.A. Zakhidov, Chem. Commun. (Cambridge) (2000) 997.
[5] P.N. Bartlett, P.R. Birkin, M.A. Ghanem, Chem. Commun. (Cambridge) (2000) 1671.
[6] R. Szamocki, S. Reculusa, S. Ravaine, P.N. Bartlett, A. Kuhn, R. Hempelmann, Angew. Chem. Int. Ed. 45 (2006) 1317.
[7] R. Szamocki, A. Velichko, C. Holzapfel, F. Muecklich, S. Ravaine, P. Garrigue, N. Sojic, R. Hempelmann, A. Kuhn, Anal. Chem. 79 (2007) 533.
[8] C.H. Wang, C. Yang, Y.Y. Song, W. Gao, X.H. Xia, Adv. Funct. Mater. 15 (2005) 1267.
[9] Y.Y. Song, Y. Li, C. Yang, X.H. Xia, Anal. Bioanal. Chem. 390 (2008) 333.
[10] J.D. Qiu, H.Z. Peng, R.P. Liang, M. Xiong, Electroanalysis 19 (2007) 1201.
[11] Y. Bai, W.W. Yang, Y. Sun, C.Q. Sun, Sens. Actuators B: Chem. 134 (2008) 471.
[12] X.J. Chen, Y.Y. Wang, J.J. Zhou, W. Yan, X.H. Li, J.J. Zhu, Anal. Chem. 80 (2008) 2133.
[13] X.H. Li, L. Dai, Y. Liu, X.J. Chen, W. Yan, L.P. Jiang, J.J. Zhu, Adv. Funct. Mater. 19 (2009) 3120.
[14] B. Serra, A.J. Reviejo, C. Parrado, J.M. Pingarron, Biosens. Bioelectron. 14 (1999) 505.
[15] N.G. Patel, A. Erlenkotter, K. Cammann, G.C. Chemnitius, Sens. Actuators B: Chem. B67 (2000) 134.
[16] R. Garjonyte, Y. Yigzaw, R. Meskys, A. Malinauskas, L. Gorton, Sens. Actuators B: Chem. 79 (2001) 33.
[17] B.D. Malhotra, A. Chaubey, Sens. Actuators B: Chem. 91 (2003) 117.
[18] S. Suman, R. Singhal, A.L. Sharma, B.D. Malthotra, C.S. Pundir, Sens. Actuators B: Chem. 107 (2005) 768.
[19] A. Parra, E. Casero, L. Vazquez, F. Pariente, E. Lorenzo, Anal. Chim. Acta 555 (2006) 308.
[20] A. Parra, E. Casero, L. Vazquez, J. Jin, F. Pariente, E. Lorenzo, Langmuir 22 (2006) 5443.
[21] M. Boujtita, M. Chapleau, N. El Murr, Electroanalysis 8 (1996) 485.
[22] S.B. Brummer, A.C. Makrides, J. Electrochem. Soc. 111 (1964) 1122.
[23] S. Ben-Ali, D.A. Cook, S.A.G. Evans, A. Thienpont, P.N. Bartlett, A. Kuhn, Electrochem. Commun. 5 (2003) 747.
[24] P.N. Bartlett, J.J. Baumberg, P.R. Birkin, M.A. Ghanem, M.C. Netti, Chem. Mater. 14 (2002) 2199.
[25] B.D. Cullity, Elements of X-ray Diffraction, 2nd ed., Addison-Wesley Publishing Company, 1978.
[26] M. Sluyters-Rehbach, J.H. Sluyters, in: A.J. Bard (Ed.), Electroanalytical Chemistry, M. Dekker, New York, 1970.
[27] R.P. Janek, W.R. Fawcett, A. Ulman, Langmuir 14 (1998) 3011.